Nonlinear Liquid Sloshing in Rectangular Tank

Tarek Uddin Mohammed [1] and Pennung Warnitchai [2]

Abstract

Nonlinear analytical solution of liquid sloshing behavior in rigid rectangular tank is presented here. Theory of perturbation with the concept of velocity potential is applied to formulate the analytical solutions. The analytical procedure transforms the nonlinear problem into a multi-stage linear problem in such a way that the solution is efficiently and easily obtained in consecutive manner. Closed form solutions for velocity potential function, free surface shape, sloshing force and wave breaking are formulated for a sinusoidal horizontal excitation along the length of the tank. Significant participation of the second sloshing mode is observed in addition to the first sloshing mode when the excitation frequency is near to the first sloshing mode or when the excitation amplitude is relatively high. It results significant deviation between upward and downward movements of free surface. The solution also indicates the phenomenon of super-harmonic resonance. Extensive shaking table experiments were carried out on a rectangular tank with different depths of water to verify the analytical solutions and also to observe the nonlinear phenomenon visually. Free surface shape, time record and frequency response of sloshing amplitude and sloshing force, wave breaking length were carefully measured and compared with the solution. It is found that the experimental results agree reasonably well with the analytical solution.

Keywords: Liquid sloshing; Tuned Liquid Damper; Harmonic ground motion; Free surface shape; Sloshing force; Wave breaking

Introduction

The understanding of liquid sloshing behavior in moving tanks is essential for many engineering applications, such as the seismic response analysis of the elevated water tanks, stability assurance of aerospace vehicles carrying liquid fuel, and also the design of Tuned Liquid Damper (TLD) to suppress the vibration of towers (Housner 1963, Abramson et al. 1966 and Qian et al. 1993).

Several analytical solutions of liquid sloshing behavior were formulated since 1960. The solutions can be grouped as linear and nonlinear depending on the considerations of free surface conditions. Linear hydrodynamic models for specific tank geometries were formulated satisfying velocity potential function with linear free surface conditions as well as tank boundary conditions (Bauer 1966). Linear solution of liquid sloshing was also obtained adopting a generalized coordinate with the potential flow theory (Tospol 1993). Linear mechanical analogy model was also developed representing the system as a linear spring mass mechanical model (Housner 1963). The linear solution represents the free surface shape as a cosine function. It also consists primary modes only. However, the linear solution cannot be applied for a moderate to large sloshing amplitude, which is most likely to develop for an excitation frequency in the neighborhood of the resonant frequency, or for large excitation amplitudes. For these reasons, the free surface shape will no longer be a cosine shape due to the significant effect of nonlinear free surface condition. Therefore, the nonlinear solution of liquid sloshing behavior is necessary for accurate representation of water sloshing in tanks.

The consideration of nonlinear free surface condition complicates the analytical procedure. As a result, the exact solutions have not yet been developed. Several nonlinear investigations were carried out to explain nonlinear behavior of liquid sloshing (Abramson et al. 1966). An approximate nonlinear solution for liquid sloshing in moving rigid tanks with harmonic excitations was also formulated (Bauer 1967).

Received 9 June 2005, Accepted 29 March 2006
[1]Associate Professor, Department of Civil Engineering, The University of Asia Pacific, Dhaka
Email: tarek@uap-bd.edu

[2]Professor, Department of Civil Engineering, Asian Institute of Technology, Bangkok, Thailand

Approximate nonlinear solution for liquid flow in an oscillating channel during earthquakes was also formulated with a semi-analytical (combination of analytical and numerical process) process (Tahara & Chwang 1993). From these review, it was understood that liquid sloshing problem is limited to its linear solution or approximate nonlinear solutions. Further study on the behavior of nonlinear liquid sloshing is still necessary in order to grasp it in a physically meaningful way.

In this study, closed form solutions were formulated for liquid sloshing in rectangular tank satisfying continuity equation with nonlinear free surface condition and other tank boundary conditions as well. Free surface shape, time history and frequency response of sloshing amplitude and sloshing force, super-harmonic resonance and wave breaking can be explained based on the analytical formulations. Finally, theoretical predictions were verified with extensive shaking table experiments.

Analytical Formulations

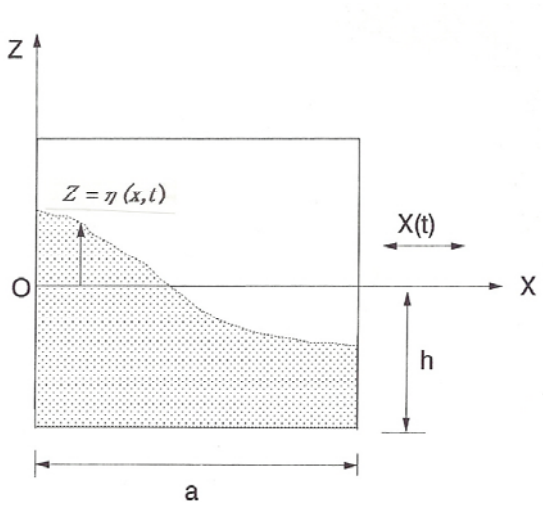

Fig. 1 Liquid sloshing in a rectangular tank

Assumptions

A rigid rectangular tank of length 'a' and quiescent liquid depth 'h' as shown in Fig. 1 is considered. The liquid in the tank is

assumed to be incompressible and inviscid. The motion of the liquid in the tank is assumed to be two dimensional and irrotational. The effect of surface tension is assumed to be negligible. A local Cartesian coordinate (X-O-Z) system is attached at the left-side tank wall such that $z = 0$ represents the quiescent free liquid surface. The free sloshing surface is defined by $z = \eta(x,t)$.

Basic Equations

The velocity of the liquid particle relative to the tank can be represented by a gradient of velocity potential function Velocity potential function is necessary to satisfy the following Laplace equation:

$$\frac{\partial^2\phi}{\partial x^2}+\frac{\partial^2\phi}{\partial z^2}=0 \text{ for } 0 \le x \le a \text{ and } -h \le z \le \eta \quad (1)$$

The kinematical boundary conditions are mentioned below:

$$u(x,z,t)=\frac{\partial\phi}{\partial x}=0 \text{ at } x=0 \text{ and } x=a \quad (2a)$$

(boundary conditions at ends of the tank)

$$w(x,z,t)=\frac{\partial\phi}{\partial z}=0 \text{ at } z=-h \quad (2b)$$

(boundary condition at bottom of the tank)

where $u(x,z,t)$ and $w(x,z,t)$ are the x and z components of liquid velocity relative to the tank at point (x,z) and time t.

The nonlinear kinematical free surface condition can be expressed as below (Bauer 1967):

$$\frac{\partial\eta}{\partial t}+\left[\frac{\partial\phi}{\partial x}\right]_{z=\eta}\frac{\partial\eta}{\partial x}=\left[\frac{\partial\phi}{\partial z}\right]_{z=\eta} \quad (3)$$

The fluid pressure $P(x,z,t)$ can be represented as below based on the Bernoulli's pressure equation (Tospol 1993) for excitation in the +ve x-direction:

$$P=-\rho\frac{\partial\phi}{\partial x}-\frac{1}{2}\rho\left[\left(\frac{\partial\phi}{\partial x}\right)^2+\left(\frac{\partial\phi}{\partial z}\right)^2\right]-\rho gz-\rho\left(x-\frac{a}{2}\right)\ddot{X} \quad (4)$$

At the free fluid surface, the fluid pressure is taken to be zero, which leads to the dynamic free surface condition as

$$\left(\frac{\partial\phi}{\partial t}\right)+\frac{1}{2}\left[\left(\frac{\partial\phi}{\partial x}\right)^2+\left(\frac{\partial\phi}{\partial z}\right)^2\right]_{z=\eta}+g\eta+\left(x-\frac{a}{2}\right)\ddot{X}=0 \quad (5)$$

Where g and $\ddot{X}$ represent the acceleration due to the gravity and the horizontal input acceleration to the rigid tank respectively. It is clear form this equation that the dynamic free surface condition is also nonlinear.

Now to obtain the analytical solutions of velocity potential function (ϕ) as well as free surface shape (η), it is necessary to satisfy the continuity equations (Eq. 1) with rigid boundary conditions (Eq. 2), nonlinear kinematic and dynamic free surface conditions (Eqs. 3 and 5).

Formulation of the Governing Equations

Here, the second order perturbation method is applied in order to reduce the complexity of the solution process attributed to the consideration of nonlinear free surface conditions. Free surface and velocity potential function can be represented in series forms with a perturbed parameter ε ($0 < \varepsilon << 1$) as below:

$$\eta(x,t)=\varepsilon^1\eta_1+\varepsilon^2\eta_2+... \quad (6)$$

$$\phi(x,z,t)=\varepsilon^1\phi_1+\varepsilon^2\phi_2+... \quad (7)$$

Substituting Eqs. 6 and 7 into Eq. 3 and applying Taylor's series of expansion and finally equating ε^1 and ε^2 terms from both sides, the following equations can be obtained:

$$\frac{\partial\eta_1}{\partial t}=\frac{\partial\phi_1}{\partial z}, \quad \text{at } z=0 \quad (8)$$

$$\frac{\partial\eta_2}{\partial t}=-\frac{\partial\phi_1}{\partial x}\frac{\partial\eta_1}{\partial x}+\eta_1\frac{\partial^2\phi_1}{\partial z^2}+\frac{\partial\phi_2}{\partial z}, \quad \text{at z=0} \quad (9)$$

Similarly, from Eqs. 5, 6 and 5, the following two equations can be derived considering $\ddot{X}$ is in the order of ε^1:

$$\frac{\partial\phi_1}{\partial t}+g\eta_1+\left(x-\frac{a}{2}\right)\ddot{X}=0, \quad \text{at z=0} \quad (10)$$

$$\frac{\partial\phi_2}{\partial t}+g\eta_2=-\eta_1\frac{\partial^2\phi_1}{\partial t\partial z}-\frac{1}{2}\left[\left(\frac{\partial\phi_1}{\partial x}\right)^2+\left(\frac{\partial\phi_1}{\partial z}\right)^2\right], \quad \text{at z=0} \quad (11)$$

Combining Eqs. 8 and 10, the following equation can be obtained with one unknown ϕ_1:

$$\frac{\partial^2\phi_1}{\partial t^2}+g\frac{\partial\phi_1}{\partial z}=-\left(x-\frac{a}{2}\right)\dddot{X}, \quad \text{at} \quad \text{z=0} \quad (12)$$

This equation is the governing equation for the first order solution i.e., the linear solution. Similarly Eqs. 9 and 11 can be combined as

$$\frac{\partial^2\phi_2}{\partial t^2}+g\frac{\partial\phi_2}{\partial z}=g\frac{\partial\phi_1}{\partial x}\frac{\partial\eta_1}{\partial x}-g\eta_1\frac{\partial^2\phi_1}{\partial z^2}-\frac{\partial\eta_1}{\partial t}\frac{\partial^2\phi_1}{\partial t\partial z}-$$

$$\eta_1\frac{\partial^3\phi_1}{\partial^2 t\partial z}-\frac{\partial\phi_1}{\partial x}\frac{\partial^2\phi_1}{\partial x\partial t}-\frac{\partial\phi_1}{\partial z}\frac{\partial^2\phi_1}{\partial z\partial t}, \quad \text{at z=0} \quad (13)$$

The above equation is the governing equation for the second order solution. If the first order solutions for are known functions, then the right hand side becomes a known force function.

First Order Solution

From Eqs. 1 and 2, the velocity potential function can be represented in terms of the time and space function as below (Mohammed 1994):

$$\phi_1(x,z,t)=\sum_{n=1}^{\infty}\dot{A}_n(t)\cosh\left(\frac{n\pi}{a}(z+h)\right)\cos\left(\frac{n\pi x}{a}\right) \quad (14)$$

Where, $\dot{A}_n(t)$ represent the derivative of an arbitrary time function. Substituting Eq. 14 into 12, and expanding $\left(x-\frac{a}{2}\right)$ in Fourier series, the following equation can be obtained:

$$\sum_{n=1}^{\infty}\dddot{A}_n(t)\cosh\left(\frac{n\pi h}{a}\right)\cos\left(\frac{n\pi x}{a}\right)+$$

$$g\sum_{n=1}^{\infty}\dot{A}_n\left(\frac{n\pi}{a}\right)\sinh\left(\frac{n\pi h}{a}\right)\cos\left(\frac{n\pi x}{a}\right)=$$

$$\left(\frac{4a}{\pi^2}\right)\sum_{n=1}^{\infty}\left(\frac{1-\cos(n\pi)}{2}\right)\frac{\cos\left(\frac{n\pi x}{a}\right)}{n^2}\ddot{X} \tag{15}$$

Integrating with respect to t and multiplying by $\cos\left(\frac{j\pi x}{a}\right)$, and again integrating with respect to x (limit $x = 0$ to a) to eliminate the terms of x and considering a specific loading function $X = X_0 \cos(\Omega t)$, the following equation can be obtained:

$$\ddot{A}_n + \omega_n^2 A_n = F_n \cos(\Omega t) \tag{16}$$

where, $\omega_n^2 = \left(\frac{n\pi g}{a}\right)\tanh\left(\frac{n\pi h}{a}\right)$ and

$F_n = (4\,a/n^2\pi^2)\,[\cos(n\pi) - 1]/(2\cos(n\pi h/a)]\,X_0\,\Omega^2$

Here, the term ω_n represents the natural frequency of the n^{th} sloshing mode. The steady state solution of Eq. 14 is

$$A_n = \frac{F_n}{\omega_n^2 - \Omega^2}\cos(\Omega t) \tag{17}$$

Substituting Eq. 17 into Eq. 14, the following equation can be obtained

$$\phi_1(x,z,t) = \sum_{n=1}^{\infty} -\frac{F_n \Omega}{\omega_n^2 - \Omega^2}\cosh\left(\frac{n\pi}{a}(z+h)\right)\cos\left(\frac{n\pi x}{a}\right)\sin(\Omega t) \tag{18}$$

Substituting Eq. 18 into Eq. 8 and integrating with respect to t, the following equation can be obtained:

$$\eta_1(x,t) = \sum_{n=1}^{\infty}\frac{F_n}{\omega_n^2 - \Omega^2}\left(\frac{n\pi}{a}\right)\sinh\left(\frac{n\pi h}{a}\right)\cos\left(\frac{n\pi x}{a}\right)\cos(\Omega t) \tag{19}$$

Here, ϕ_1 and η_1 represent the linear solutions for the velocity potential function and free surface shape.

Second Order Solution

Like the first order solution, consider ϕ_2 as

$$\phi_2(x,z,t) = \sum_{n=1}^{\infty}\dot{B}n(t)\cosh\left(\frac{n\pi}{a}(z+h)\right)\cos\left(\frac{n\pi x}{a}\right) \tag{20}$$

Here, $\dot{B}_n(t)$ is considered as the derivative of an arbitrary time function to obtain second order solution. Substituting Eqs. 18, 19 and 20 into Eq. 13 and integrating with respect to t, the following equation can be obtained:

$$\sum_{n=1}^{\infty}\ddot{B}_n Ch_n Co_n + \sum_{n=1}^{\infty} B_n \tilde{n} Sh_n Co_n =$$
$$D(t)\sum_{n=1}^{\infty}\sum_{k=1}^{\infty} C_{nk}\tilde{n}\tilde{k}\left(Ch_n Sh_k Si_n Si_k g - \tilde{k} Sh_n Ch_k Co_n Co_k g + 3\Omega^2 Sh_n Sh_k Co_n Co_k + \Omega^2 Ch_n Ch_k Si_n Si_k\right) \tag{21}$$

where,

$Ch_n = \cosh\left(\frac{n\pi h}{a}\right)$, $Co_n = \cos\left(\frac{n\pi x}{a}\right)$, $Ch_k = \cosh\left(\frac{k\pi h}{a}\right)$,

$Co_k = \cos\left(\frac{k\pi x}{a}\right)$, $Sh_n = \sinh\left(\frac{n\pi h}{a}\right)$

$Si_n = \sin\left(\frac{n\pi x}{a}\right)$, $Sh_k = \sinh\left(\frac{k\pi h}{a}\right)$, $\mathrm{Si_k} = \sin\left(\frac{\mathrm{k}\pi \mathrm{x}}{\mathrm{a}}\right)$,

$\tilde{n} = \frac{n\pi}{a}$, $\tilde{k} = \frac{k\pi}{a}$,

$C_{nk} = \frac{F_n F_k}{\left(\omega_n^2 - \Omega^2\right)\left(\omega_k^2 - \Omega^2\right)}$, and $D(t) = \frac{1}{4}\cos(2\Omega t)$

To eliminate x, multiply by $\cos\left(\frac{j\pi x}{a}\right)$ to the both sides and integrating with respect to x (limit of $x = 0$ to a). For $n = 1$ and $k = 1$ and also for excitation frequency (Ω) close to the first mode frequency, the right hand side of the above equation will be significant. Considering these situations and also using the orthogonality of the trigonometric function, the following equation can be obtained:

$$\ddot{B}2 + \omega_2^2 B_2 = Q(h,a,X_O,\Omega)\cos(2\Omega t) \tag{22}$$

where,

$$Q(h,a,X_O,\Omega) = \frac{1}{8Cosh\left(\frac{2\pi h}{a}\right)}\left(\frac{\pi}{a}\right)^2 C_{11}\left(-\frac{\pi}{a}Sinh\left(\frac{2\pi h}{a}\right)g + 2\Omega^2 Sinh^2\left(\frac{\pi h}{a}\right) - \Omega^2\right)$$

Eq. (22) represents the equation of motion for the second order solution. The steady state solution of this equation can be written as:

$$B_2 = Q(h,a,X_O,\Omega)\frac{1}{\left(\omega_2^2 - 4\Omega^2\right)}\cos(2\Omega t) \tag{23}$$

Substituting Eq. 23 into Eq. 20, the following equation is obtained:

$$\phi_2(x,z,t) = Q(h,a,X_O,\Omega)\frac{2\Omega}{\left(4\Omega^2 - \omega_2^2\right)}\cosh\left(\frac{2\pi}{a}(z+h)\right)\cos\left(\frac{2\pi x}{a}\right)\sin(2\Omega t) \tag{24}$$

Substituting Eqs. 18, 19 and 24 into Eq. 9 and integrating with respect to t, the following equation can be obtained:

$$\eta_2(x,t) = \frac{1}{4}\frac{F_1^2}{\left(\omega_1^2 - \Omega^2\right)}\cosh\left(\frac{\pi h}{a}\right)\sinh\left(\frac{\pi h}{a}\right)\left(\frac{\pi}{a}\right)^3\cos\left(\frac{2\pi x}{a}\right)\cos(2\Omega t) + Q(h,a,X_O,\Omega)\frac{1}{\left(\omega_2^2 - 4\Omega^2\right)}\sinh\left(\frac{2\pi h}{a}\right)\left(\frac{2\pi}{a}\right)\cos\left(\frac{2\pi x}{a}\right)\cos(2\Omega t) \tag{25}$$

Where, ϕ_2 and η_2 are the contributions of the nonlinear effects.

Combined Solutions

Substituting Eqs. 18 and 24 into Eq. 7, the following equation can be obtained:

$$\phi(x,z,t) = \sum_{n=1}^{\infty} -\frac{F_1\Omega}{(\omega_n^2 - \Omega^2)}\cosh\left(\frac{n\pi}{a}(z+h)\right)\cos\left(\frac{n\pi x}{a}\right)\sin(\Omega t) + Q(h,a,X_O,\Omega)\frac{2\Omega}{(2\Omega)^2 - \omega_2^2}\cosh\left(\frac{2\pi}{a}(z+h)\right)\cos\left(\frac{2\pi x}{a}\right)\sin(2\Omega t) \tag{26}$$

The first term of the above-equation represents the linear part

of the velocity potential function and the second part represents the additional part due to the consideration of the nonlinear free surface conditions. This term will give significant contribution when the excitation frequency is near the half of the second sloshing mode. This is known as super-harmonic resonance.

Substituting Eqs. 19 and 25 into Eq. 6, the following equation can be obtained:

$$\eta(x,t)=\frac{F_1}{\left(\omega_1^2-\Omega^2\right)}\left(\frac{\pi}{a}\right)\sinh\left(\frac{\pi h}{a}\right)\cos\left(\frac{\pi x}{a}\right)\cos(\Omega t)+$$

$$\frac{1}{4}\frac{F_1^2}{\left(\omega_1^2-\Omega^2\right)}\cosh\left(\frac{\pi h}{a}\right)\sinh\left(\frac{\pi h}{a}\right)\left(\frac{\pi}{a}\right)^3\cos\left(\frac{2\pi x}{a}\right)\cos(2\Omega t)+$$

$$Q(h,a,X_O,\Omega)\frac{1}{\left(\omega_2^2-4\Omega^2\right)}\left(\frac{2\pi}{a}\right)\sinh\left(\frac{2\pi h}{a}\right)\cos\left(\frac{2\pi x}{a}\right)\cos(2\Omega t) \quad (27)$$

Eq. (27) shows that the free surface is the combination of three terms. The first term is the linear part. The other terms are the additional terms due to the considerations of nonlinear free surface conditions. The second term will be significant near the resonance frequency and also for higher excitation amplitude. The free surface is deviated from the cosine shape due to the addition of the second and third terms. The third term represents the presence of super-harmonic resonance.

Damping of pure liquid was not included in the formulations, therefore the solutions for η and ϕ become unbound at the resonance.

Sloshing Force

The sloshing force exerted on the tank wall due to the sloshing of water inside the tank can be calculated from the unsteady Bernoulli's equation of pressure (Eq. 4) as below:

$$F_S=\int_{-h}^{\eta_a} P_{x=a}b\,dz-\int_{-h}^{\eta_0} P_{x=0}b\,\mathrm{d}z \quad (28)$$

where η_a and η_0 are sloshing height at $x=a$, and $x=0$ respectively. Substituting Eqs. 5, 6 and 7 into Eq. 28, and expanding hyperbolic functions in Taylor's series and neglecting the higher order term, the sloshing force can be written as

$$F_S=\rho bahX_O\Omega^2\cos(\Omega t)\left[\frac{8a\Omega^2}{\pi^3 h\left(\Omega^2-\omega_q{}^q\right)}\tan\left(\frac{\pi h}{a}\right)-1\right]-$$

$$\rho bahX_O\Omega^2\cos(\Omega t)\left[\frac{4X_0\Omega^2}{\pi h\left(\Omega^2-\omega_1^2\right)}\cos(\Omega t)\right] \quad (29)$$

The first two terms are obtained from the first order solutions, which are the part of the linear solution. The third term is the additional term for the consideration of the nonlinear effect. Like other solutions, the sloshing force becomes unbound exactly at the resonance frequency. The effect of the super-harmonic resonance did not observe in the sloshing force equation, because the second super-harmonic condition is observed due to the strong contribution of the second mode, which does not carry any sloshing force.

Wave Breaking

During sloshing, the fluid particles will separate during the reversal of free fluid surface, if their acceleration is greater or equal to that of acceleration due to the gravity. This condition for wave breaking can be written as (Bauer 1967):

$$-\ddot{\eta}\geq g \quad (30)$$

Equation 27 can be rewritten as

$$\eta=\alpha\cos(\Omega t)\cos\left(\frac{\pi x}{a}\right)+(\beta+\gamma)\cos(2\Omega t)\cos\left(\frac{2\pi x}{a}\right) \quad (31)$$

Where, $\alpha=F_1\left(\frac{\pi}{a}\right)\sinh\left(\frac{\pi h}{a}\right)$, $\beta=\frac{Q}{\omega^2-(2\Omega)^2}\sinh\left(\frac{2\pi h}{a}\right)\left(\frac{2\pi}{a}\right)$ and

$$\gamma=\frac{1}{4}\frac{F_1^2}{\left(\omega_1^2-\Omega^2\right)}\cosh\left(\frac{\pi h}{a}\right)\sinh\left(\frac{\pi h}{a}\right)\left(\frac{\pi}{a}\right)^3$$

Substituting Eq. 31 into Eq. 30, the following equation can be obtained:

$$\alpha Cos\left(\frac{\pi x}{a}\right)+8Cos^2\left(\frac{\pi x}{a}\right)(\beta+\gamma)-4(\beta+\gamma)-\frac{g}{\Omega^2}\geq 0 \quad (32)$$

The above equation represents the wave breaking condition in the tank.

Experimental Results and Verifications

Experimental Setup

Extensive experimental investigations were carried out to verify the analytical formulations and also to observe the sloshing phenomenon visually. The detail experimental setup is shown in Fig. 2.

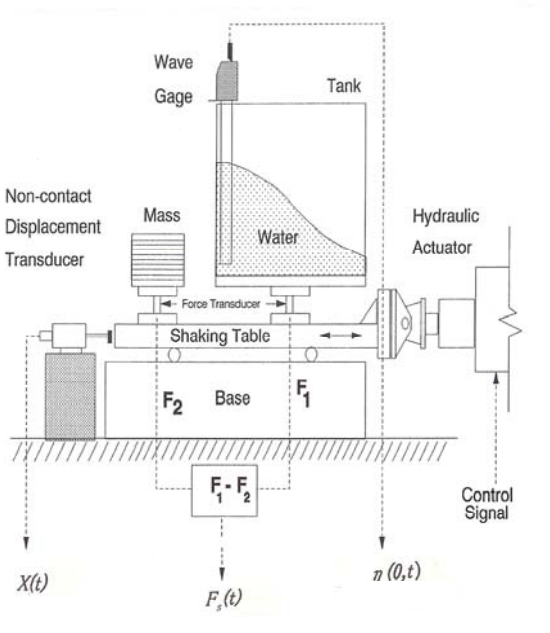

Fig. 2 Experimental setup

A rectangular acrylic transparent tank having length *a = 40* cm, width *b = 20* cm was mounted on a force transducer which was firmly fixed on the bed of a shaking table. The liquid was tap water. The transparent tank allowed the visual observation of the free surface inside the tank. Vertical and

horizontal grid lines were drawn on a side face of the tank at one cm interval to measure the free surface profile and also to check the sloshing height measured from the wave gauge. The shaking table was one-directional type and was driven by a feedback control hydraulic actuator. The table movement represented the movement of the tank *X(t)*. It was measured by a non-contact displacement transducer. The wave amplitude near the tank wall $\eta(0,t)$ was measured by a capacitance wave gauge. The force transducer was designed to sense, exclusively, the horizontal component of force acting on it top. The transducer was made of steel pipe attached with two semi-conductor strain gauges. It was very rigid and sensitive to force. Another set of force transducer with a mass identical to the tank mass was used for simulating the inertia force of the empty tank. Subtraction of these output signals yields a pure signal of liquid-sloshing force, F_s. An additional 1.5 cm rectangular plywood plate, having the same dimension of the tank bottom was coupled with the tank's bottom. The free vibration test of the empty tank assembly showed that the natural frequency of the tank was about 14 Hz, which was far away from the test frequency. Therefore, the rigid container assumption was satisfied. All signals were passed through the low pass filter with a cut-off frequency of 5 Hz, which was much higher than the interested frequency. One oscilloscope was used to observe and measure the distance between peak to peak of the output signals. An A/D conversion device was used to transfer the analogue data to digital data. All digital data were stored in a computer disk for further analysis.

Free Surface Shape

The steady state shape of the free surface for $h/a = 0.3, \mathrm{X}_0/a = 0.0025$ and $\Omega/\omega_1 = 1.05$ is shown in Fig. 3(a). The results are shown at the beginning and half of a sloshing cycle. It is found that the nodal point crossing the quiescent free surface is not fixed at the mid of the tank, it moves in between 'm' and 'n'. In this case, the free surface shape is slightly different from the regular cosine shape. The steady state free surface shape for $h/a = 0.3, \mathrm{X}_0/a = 0.0025$ and $\Omega/\omega_1 = 1.01$ is shown in Fig. 3(b). For excitation frequency very close to the natural sloshing frequency, significant difference in upward and downward movements of water is observed. Reasonable agreement between experiment and theory is observed.

Theoretical free surface shapes near super-harmonic resonance for $h/a = 0.2, \mathrm{X}_0/a = 0.005$ and $2\Omega/\omega_2 = 0.994$ are shown in Fig. 3(c) at *T=0.0, 0.25T, 0.5T, 0.75T* and *T*. It is clear that during the super-harmonic resonance, the free surface shape changes very much from the regular cosine shape of the first sloshing mode. It is happened due to the strong coupling of the second sloshing mode at this particular frequency. The observation of super-harmonic resonance was clearer for a shallow depth of water. The experimental free surface profile could not be recorded for a particular time. Therefore, only the theoretical results are explained.

Time History of Sloshing Amplitude

Time history of sloshing amplitude $\eta(0,t)$ is shown in Fig. 4(a) for $h/a = 0.3, \mathrm{X}_0/a = 0.0025$ and $\Omega/\omega_1 = 1.05$. A little difference in upward and downward movements is found. The time history of sloshing amplitude for $h/a = 0.3, \mathrm{X}_0/a = 0.0025$ and $\Omega/\omega_1 = 1.01$ is shown in Fig. 4(b). Significant difference in upward and downward movements is observed for excitation frequency close to the resonant frequency. The upward peaks are very sharp compared to the downward peaks. Reasonably good agreement was observed between theory and experiment.

The time history of sloshing amplitude $\eta(0,t)$ near super-harmonic resonance is shown in Fig. 4(c) for $h/a = 0.2, \mathrm{X}_0/a = 0.005$. Theoretical results correspond to $2\Omega/\omega_2 = 0.994$ and the experimental results correspond to $2\Omega/\omega_2 = 1.0$. During the experiment, it was found that the super-harmonic resonance was very sensitive to the excitation frequency. It could not be found at the intended frequency similar to the theory. Therefore, different excitation frequency was used in theory and experiment. A good similarity is observed between experiment and theory.

Upward and Downward Movement of Sloshing Water

The upward and downward movements of sloshing amplitude with respect to excitation amplitude are shown in Fig. 5(a) for $h/a = 0.3, \Omega/\omega_1 = 1.01$. The upward movement of sloshing water is increased with increase of excitation amplitudes. The downward movement is increased in a much slower rate compared to the upward movement. The first order solution gives the linear relationship. The average sloshing amplitudes with the variation of excitation amplitude is shown in Fig. 5(b) for $h/a = 0.3, \Omega/\omega_1 = 1.01$ and $h/a = 0.3, \Omega/\omega_1 = 1.05$.

For the excitation frequency close to the natural sloshing frequency and higher excitation amplitude ($X_o/a \geq 0.00288$) wave breaking was observed. Significant deviation between theoretical and experimental results is observed at wave breaking condition.

Frequency Response of Sloshing Height

For $h/a = 0.3, X_0/a = 0.0025$ and $h/a = 0.3, X_0/a = 0.01$, the average sloshing height amplitude with respect to excitation frequency is shown in Fig. 6. Here, the amplitude was measured at the steady state condition. Reasonably good agreement is observed between experiment and theory. Super-harmonic resonance is observed at the excitation frequency half of the second sloshing mode frequency. It was observed for a very narrow frequency band. Very clear observation of super-harmonic resonance is observed for larger excitation amplitude.

Time History of Sloshing Force

The time history of sloshing force amplitude for $h/a = 0.3, \mathrm{X}_0/a = 0.0025, \Omega/\omega_1 = 1.05$ is shown in Fig. 7(a). Positive and negative sloshing force amplitudes are equal. The experimental results coincide with the theoretical results. The time history of sloshing force amplitude for $h/a = 0.3, \mathrm{X}_0/a = 0.0025, \Omega/\omega_1 = 1.01$ is shown in Fig. 7(b). Positive and negative sloshing amplitudes are again equal. A difference is found between theory and experiment. Here, during the formulation of the equations, second order perturbation method was applied to avoid the complicacy of the solution process. For exact prediction of sloshing force, higher order perturbation is necessary.

Sloshing Force Amplitude vs. Excitation Amplitude

The sloshing force amplitude with the variation of excitation amplitude is shown in Fig. 8 for $h/a = 0.3, \Omega/\omega_1 = 1.05$ and $h/a = 0.3, \Omega/\omega_1 = 1.01$.

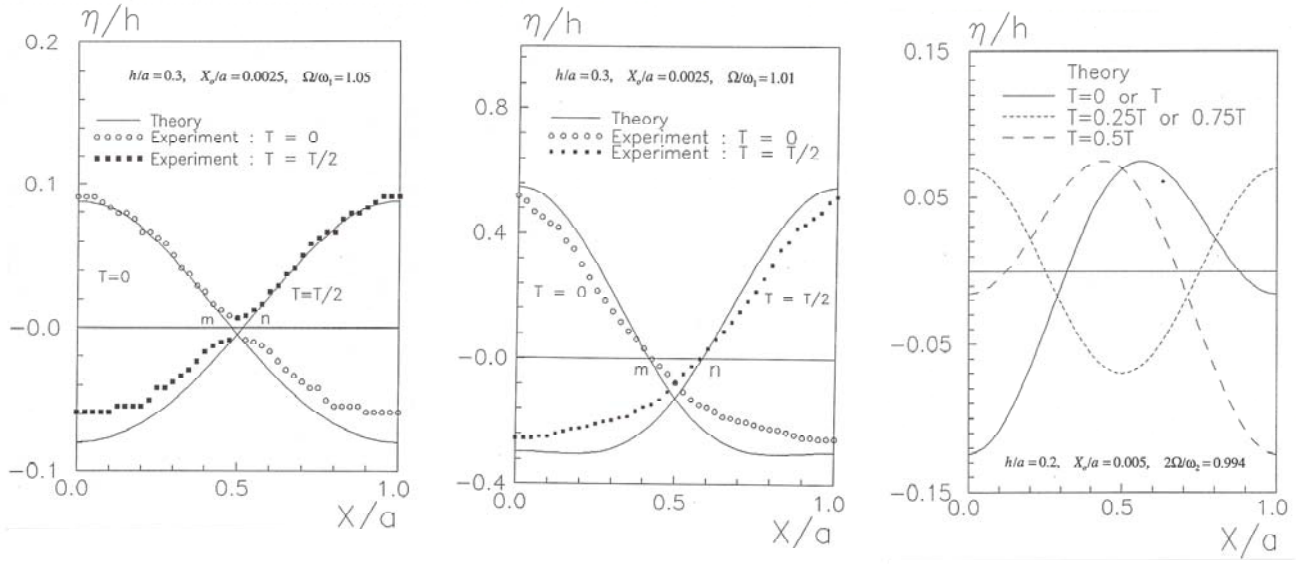

Fig. 3 Free surface shape for (a) $\Omega/\omega_1 = 1.05$, (b) $\Omega/\omega_1 = 1.01$ and (c) $2\Omega/\omega_1 = 0.994$

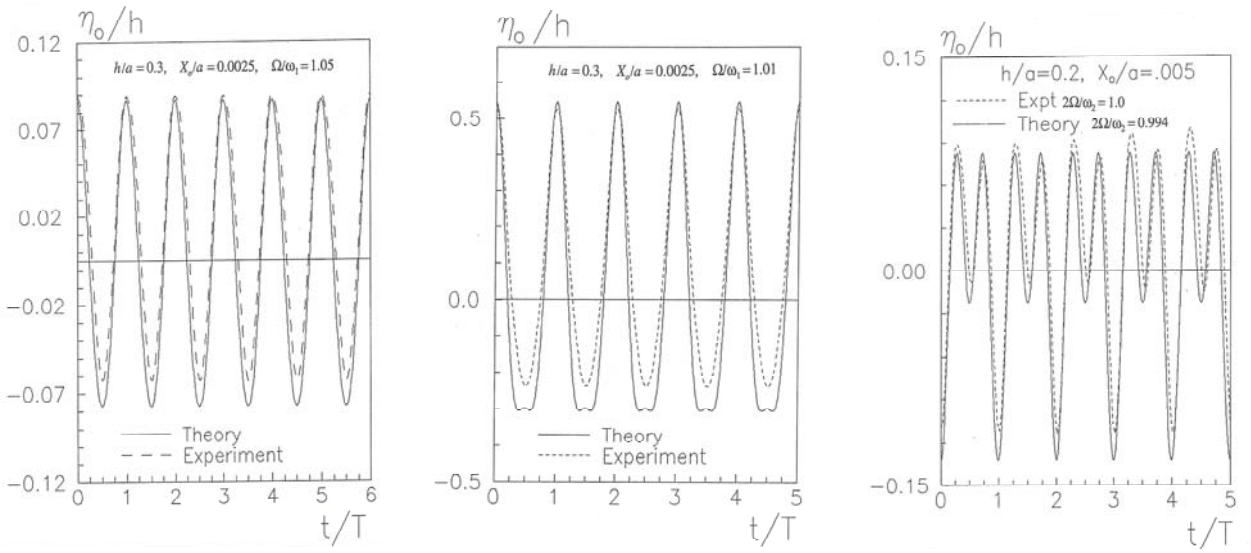

Fig. 4 Steady state response of sloshing height at the tank edge for (a) $\Omega/\omega_1 = 1.05$, (b) $\Omega/\omega_1 = 1.01$ and (c) $2\Omega/\omega_1 = 0.994$

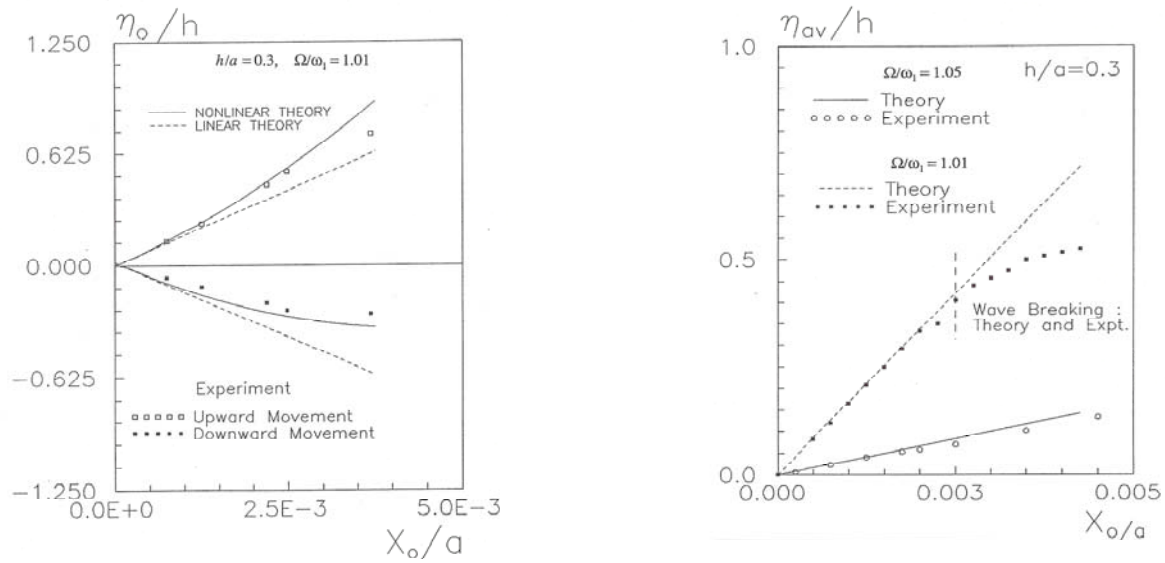

Fig. 5 (a) Upward and downward sloshing amplitude, (b) Average sloshing amplitude with the variation of excitation amplitude

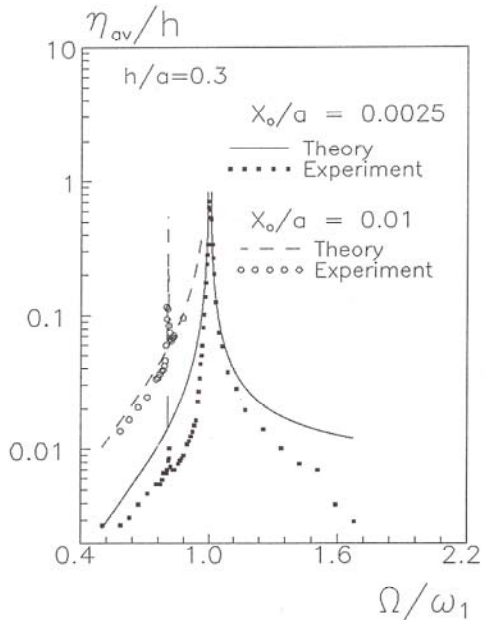

Fig. 6 Frequency response of average sloshing amplitude

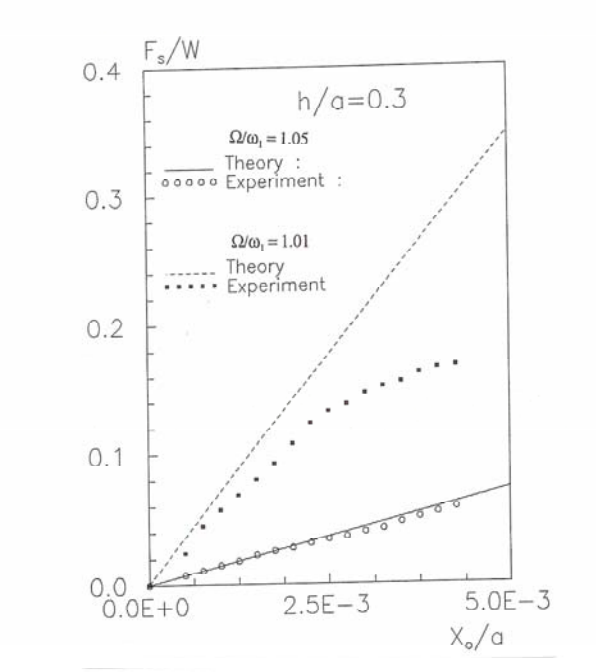

Fig. 8 Sloshing force amplitude vs. excitation amplitude

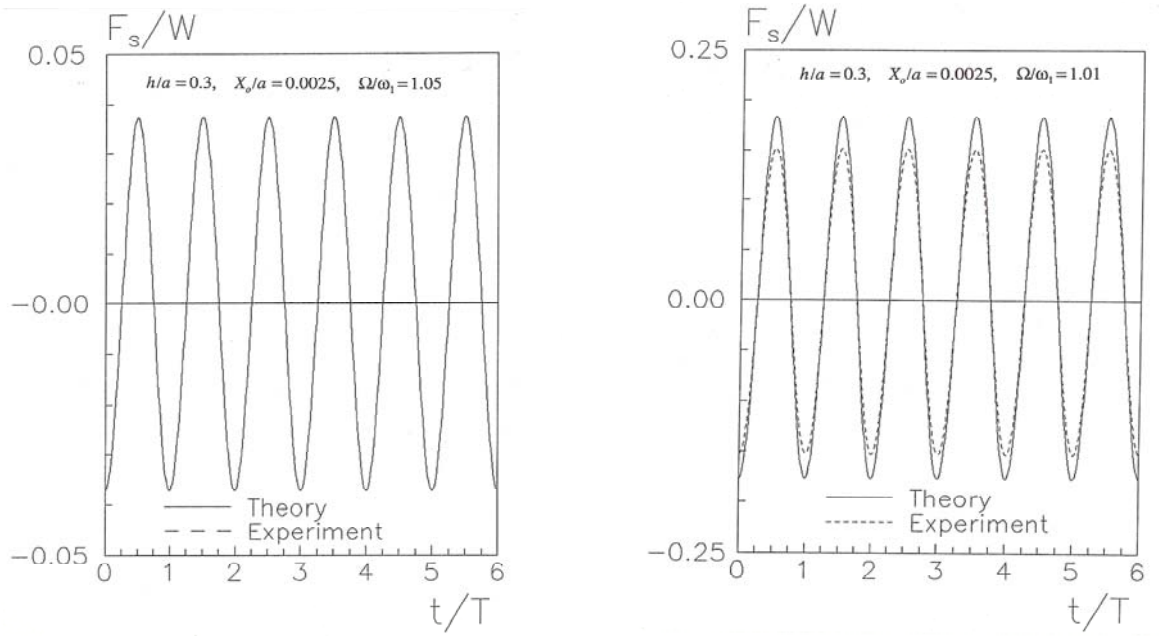

Fig. 7 Steady state response of sloshing force for (a) Ω/ω_1 = 1.05, (b) Ω/ω_1 = 1.01

For $h/a = 0.3, \Omega/\omega_1 = 1.05$, experimental results show a very good agreement with the theoretical results. For $h/a = 0.3, \Omega/\omega_1 = 1.01$, a deviation between theory and experiment is observed, especially for larger excitation amplitudes. The reason of this deviation can be explained as before.

Frequency Response of Sloshing Force Amplitude

For $h/a = 0.3, X_0/a = 0.0025$, frequency response of sloshing force amplitude is shown in Fig. 9. Good agreement is observed between theory and experiment.

The effect of super-harmonic resonance is not observed in the sloshing force amplitude as the super-harmonic mode occurs due to the strong contribution of the second sloshing mode that does not bring sloshing force.

Wave Breaking

The wave breaking length *d* (measured at the end of the tank) with excitation frequency is shown in Fig. 10. Near the resonant frequency, the wave breaking length is the highest. The frequency range for commencing the wave breaking is increased with the increase of excitation amplitude. Good agreement is observed between experiment and theory.

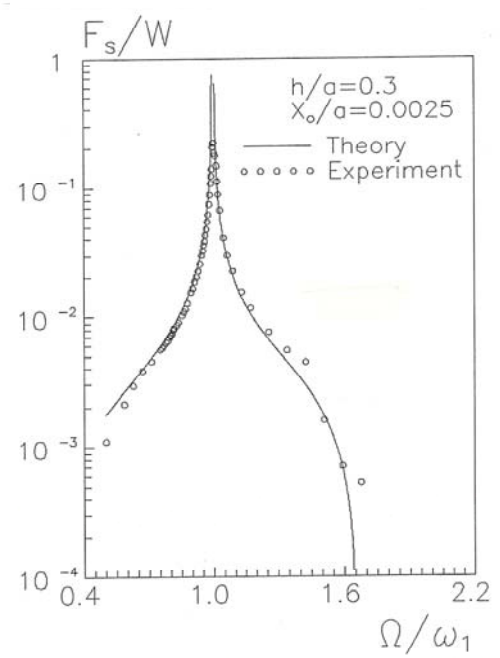

Fig. 9 Frequency Response of sloshing force amplitude

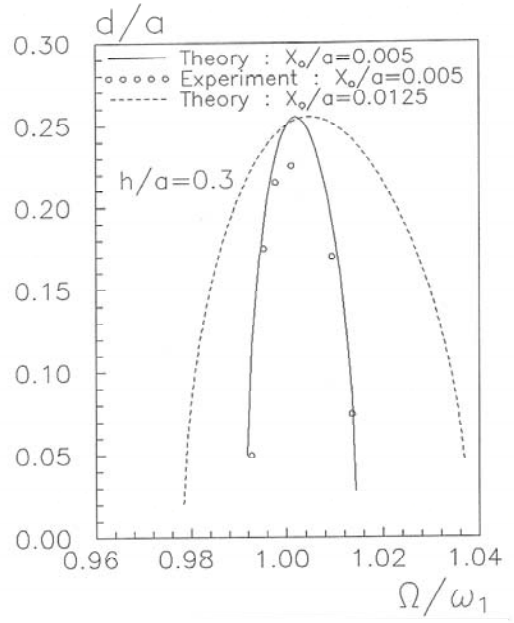

Fig. 10 Wave breaking length vs. excitation frequency

Conclusions

Closed form analytical solutions are formulated to describe the first-mode-liquid- sloshing behavior in a rectangular tank due to a sinusoidal excitation. The solutions can predict the nonlinear liquid sloshing phenomenon very close to the resonant frequency. The solutions can evaluate steady state free surface shape, the existence of super-harmonic resonance, time history and frequency response of sloshing amplitudes and sloshing force, commencement and length of wave braking. Reasonably good agreement is observed between experiment and theory.

Acknowledgment

The authors wish to express their profound gratitude and sincere appreciation to Asian Institute of Technology (AIT), Department of Civil Engineering, Bangkok, Thailand for financing the experimental works related to this study.

References

Abramson HN, Chu WH and Kana DD (1966). Some studies of nonlinear lateral sloshing in rigid containers. *ASME J. of Appl. Mech.*, 33, 777-84.

Bauer HF (1966). Response of liquid in a rectangular container. *ASCE J. of Engg. Mech.*, 92, EM6, 1-23.

Bauer HF (1967). Nonlinear propellant sloshing in a rectangular container of infinite length. *Developments in Theo. and Appl. Mech.*, Oxford: Pergaman Press, 3, 723-59.

Qian JR, Warnitchai P and Ding X (1993). Dynamic response suppression of a TV tower model by TLD: Shaking table tests. *Proc. of the EASEC-5 Intl. Conf. on Building for the 21st Century*, Ed. Look YC, Australia, 1549-54.

Housner GW (1963). The dynamic behavior of water tanks. *Bull. of the Seism. Soc. of America*, 53(2), 381-7.

Mohammed TU (1994). A study of nonlinear liquid sloshing in rectangular tanks for damper application. *Masters Thesis*, Dept. of Civil Engg., Asian Institute of Technology, Bangkok, Thailand.

Tahara Y and Chwang T (1993). Nonlinear free-surface flow in oscillating channel during earthquakes. *ASCE J. of Engg. Mech.*, 119(4), 801-12.

Tospol P (1993). Analytical model of liquid sloshing for Tuned Liquid Damper application. *Masters Thesis*, Dept. of Civil Engg., Asian Institute of Technology, Bangkok, Thailand.